CHEMICAL MODIFICATION OF Al_2O_3 NANOPARTICLES BY PMMA VIA A FACILE SURFACE INITIATED CONTROLED RADICAL POLYMERIZATION

M. R. Islam, L. G. Bach, T. B. Mai, T. T. Nga, L. Niranjanmurthi, K. T. Lim*

Department of Imaging System Engineering, Pukyong National University, Busan, 608-737, Korea
** E-mail address: ktlim@pknu.ac.kr (K.T. Lim).*

Keywords: PMMA-*g*-Al_2O_3 nanocomposites, grafting from, surface initiated controlled radical polymerization.

Abstract
Organic-inorganic hybrid nanocomposites composed of poly(methyl methacrylate) and Al_2O_3 nanoparticles (PMMA-g-Al_2O_3) were prepared through a facile surface thiol-lactam initiated radical polymerization (TLIRP) using grafting from strategy. The surface of Al_2O_3 nanoparticles (Al_2O_3 NPs*) was modified by (3-mercapto)propyl trimethoxysilane in order to prepare thiol functionalized Al_2O_3 NPs (Al_2O_3-SH). A controlled radical polymerization of MMA was conducted to afford covalently bonded PMMA with* Al_2O_3 NPs *in the presence of Al_2O_3-SH and butyrolactam. The surface functionalization, bonding nature, morphologies, thermal and physical structure of PMMA-g-Al_2O_3 nanocomposites were investigated by FT-IR, XPS, EDS, SEM, TGA, DSC and DLS analyses. The controlled nature of the TLIRP of MMA from the surface of Al_2O_3-SH was ascertained by GPC analysis.*

1 Introduction

Over the few decades, a variety of new hybrid materials for engineering and biological applications through different techniques have been developed. Due to their nanometer scale size, nanomaterials demonstrate unique physicochemical properties, thus successfully applied in the areas of catalysis, electrochemistry, drug delivery, and optoelectronics [1]. Recently, hybrid materials based on polymers with nanoscaled inorganic fillers have gained immense interests because of the integration of the functionality and processibility of an organic phase and enhanced thermal/chemical stability of an inorganic phase. Much work has already been accomplished on the incorporation of inorganic materials such as SiO_2, TiO_2, Fe_3O_4, $Mg(OH)_2$ in polymer matrices [2,3]. On the contrary, only a few studies were conducted on the polymeric composites of Al_2O_3. Although Al_2O_3 nanoparticles (Al_2O_3 NPs) is one of the major and frequently used engineered oxide nanoparticles with significant industrial potential applications such as good biocompatibility, chemical stability, catalyst, electrical insulation, and corrosion resistance. However, because of nanoscale size Al_2O_3 NPs suffer from easy agglomeration due to its high surface energy resulting in frustrating physico-chemical properties. Thus, appropriate encapsulation of Al_2O_3 NPs by polymer will alleviate the existing bottlenecks.

Basically, there are two basic routes to deposit polymer on solid surface; one is physical adsorption and another is chemisorptions method. Covalently bonded polymers can usually

overcome drawbacks of that prepared by physical adsorption, such as low grafting densities and low adhesive forces [4,5]. Nowadays, the controlled radical polymerization methods are widely used for surface modification of nanoparticles. However, most of these techniques require many reaction steps and/or it is difficult to remove metallic catalyst completely from the final product [6-8]. Surface bound thiol groups can be used as chain transfer agents because of their high chain transfer constant. The silane coupling reagent, 3-mercaptopropyl-trimethoxysilane (MPTMS), is used to prepare thiol-terminated silica. Ultra thin polymer films could be prepared *via* a surface chain-transfer reaction [9]. Recently, we observed that thiol group can initiate polymerization with the aid of butyrolactam (BL) [10-12].

It is our great delight that the covalently bonded Al_2O_3 NPs with poly (methyl methacrylate) (PMMA) was successfully realized by a simple surface functionalized thiol-lactam initiated radical polymerization (TLIRP) applying *grafting from* strategy. Initially, Al_2O_3 NPs were functionalized with MPTMS to afford thiol immobilized Al_2O_3 (Al_2O_3-SH). Subsequently, a controlled radical polymerization of MMA with a two component initiating system comprised of Al_2O_3-SH and BL efficiently resulted PMMA-*g*-Al_2O_3 nanocomposites.

2 Materials and testing methods

2.1 Materials

Aluminium oxide (Al_2O_3) nanoparticles, (3-mercaptopropyl)trimethoxysilane (MPTMS), butyrolactam (BL) and all solvents were used as received. Methyl methacrylate (MMA) was purified by passing the liquid through a neutral alumina column to remove the inhibitor prior to use. All of the above chemicals were purchased from Aldrich, Yongin, Korea.

2.2 Grafting of MPTMS onto Al_2O_3 NPs (Al_2O_3-SH)

In a typical procedure, 4.0 g Al_2O_3 nanoparticles were added into a mixture of 4.0 g MPTMS and 50 mL THF. The resulting colloidal suspension was ultrasonically stirred for one hour and precipitated by sedimentation at room temperature. The precipitated nanoparticles were rinsed with THF to remove the excessive MPTMS and dried completely in a vacuum oven at at 40 ^oC for overnight.

2.3 Synthesis of PMMA-g-Al_2O_3 nanocomposites by TLIRP

A typical procedure for synthesis of PMMA-*g*-Al_2O_3 nanocomposites as follows: 1.0 g of MMA, 0.2 g of Al_2O_3-SH, 0.1 g of BL, 2 mL of toluene and a Teflon-coated stir bar were placed in a 25 mL round flask equipped with a reflux condenser. The flask was purged with nitrogen, heated to 80 ^oC and kept stirring. By the end of the reaction, the viscosity increased dramatically. After the desired time, the flask was cooled to room temperature and the reaction mixture was precipitated in hexane. The PMMA-*g*-Al_2O_3 nanocomposites were washed with toluene and vacuum filtered using sintered glass and dried overnight at 40 ^oC.
To investigate the dependency of number average molecular weight (M_n) and polydispersity index (PDI = M_w/M_n) of the grafted PMMA with reaction time, PMMA brushes were cleaved from the Al_2O_3 surface in the following way: 100 mg of the PMMA-*g*-Al_2O_3 were dissolved in 1 mL of HCl (2 M) and 10 mL of THF. The solution was allowed to stir at 80 ^oC under reflux for 24 h. The cleaved PMMA in the organic layer was precipitated in hexane.

2.4 Instrumentation

Fourier-transformed infrared spectrophotometry (FT-IR) was used to characterize the change in the surface functionalities of Al_2O_3 using a BOMEM Hartman & Braun FT-IR spectrometer. Surface composition was investigated using X-ray Photoelectron Spectroscopy (XPS) (Thermo VG Multilab 2000). GPC was performed by an Agilent 1200 Series equipped

(PLgel 5 μm MIXED-C columns), with THF as the solvent. Calibration was carried out using PMMA standards. The physical structure of the functionalized Al_2O_3 NPs was determined by a Philips X'pert-MPD system diffractometer (Netherlands). The morphology of the hybrids was captured by using Field Emission Scanning Electron Microscopy (FE-SEM, Hitachi JEOL- JSM-6700F). The hydrodynamic diameter was determined by the Brookhaven BI-200SM light scattering system. Thermogravimetric analysis (TGA) was conducted with Perkin-Elmer Pyris 1 analyzer (USA). The differential scanning calorimetry (DSC) measurements were undertaken using a Perkin Elmer calorimeter (DSC6200).

3 Results and discussion

3.1 Immobilization of MPTMS onto Al_2O_3 NPs via coupling reaction

In order to obtain the PMMA-*g*-Al_2O_3 nanocomposites *via* TLIRP, it is necessary to immobilize the thiol group on the Al_2O_3 NPs (Al_2O_3-SH) to act as chain transfer agent. Al_2O_3-SH was afforded *via* ligand-exchanging reaction between the hydroxyl groups on the surface of Al_2O_3 NPs and triethoxyliane groups of MPTMS to form Al–O–Si bonding linkages. The covalent bond formation between MPTMS and the Al_2O_3 NPs was confirmed by FT-IR analysis. In the spectrum of as received Al_2O_3 NPs, the strong absorption band at 3467 cm^{-1} is attributed to hydroxyl stretching and band at 1637 cm^{-1} is due to –OH bending. After surface modification with MPTMS, an S–H stretching band at 2572 cm^{-1}, asymmetric and symmetric $–CH_2$ stretching vibrations appeared at 2923 and 2857 cm^{-1}, respectively. From these results, it can be revealed that the MPTMS coupling agent was grafted on the surface of Al_2O_3 NPs through the formation of covalent bond.

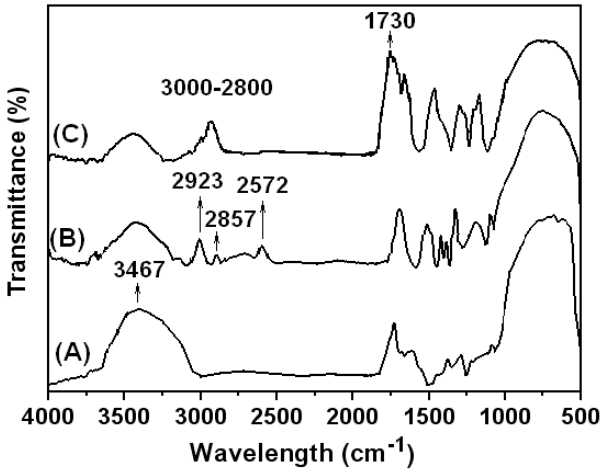

Figure 1. FT-IR spectra of (A) Al_2O_3 NPs, (B) Al_2O_3-SH, and (C) PMMA-*g*-Al_2O_3 nanocomposites.

XPS was used to analyze the surface chemical composition of Al_2O_3-SH. Figure 2A shows the XPS spectrum of the Al_2O_3 NPs surface which is dominated by signals attributable to O, Al, and C. The XPS analysis of Al_2O_3-SH confirms the immobilization of initiator on the surface of Al_2O_3 NPs. The characteristic signals for oxygen (O1s at 530.8 eV), carbon (C1s at 285.2 eV), sulfur (S2p at 163.4 eV), silicon (Si2p at 101.6 eV) and aluminum (Al2p at 73.6 eV), are clearly observed in the wide scan spectrum (Figure 2B). Silane coupling agent immobilized on surface Al_2O_3 NPs can facilitate a condensation reaction with MPTMS to produce a stable initiator monolayer, consistent with the appearance of the Si, S core-level signals in the wide-scan spectrum of Al_2O_3-SH surface. In addition, the elemental mapping analysis of the Al_2O_3-SH was further investigated by EDX as shown in Figure 2D. The characteristic peaks ascribed to Al, Si, C, O and S elements are present in the EDX spectrum which suggests that the MPTMS was immobilized onto the Al_2O_3 NPs.

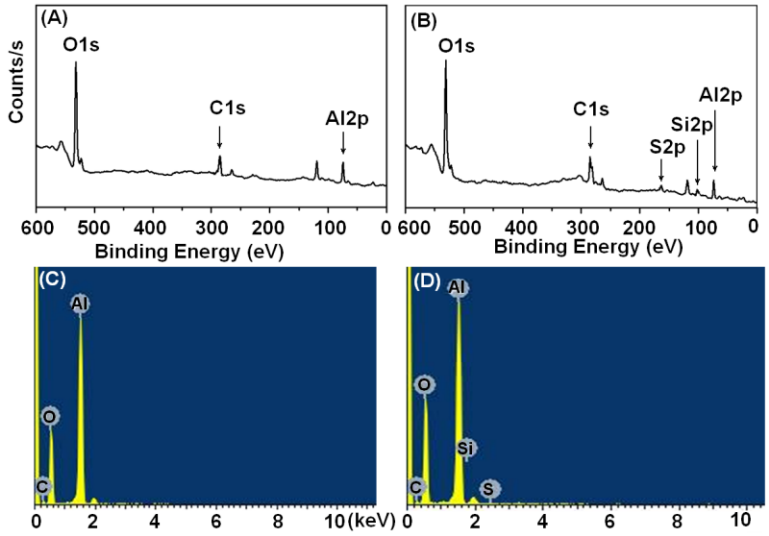

Figure 2. (A,B) Wide-scan spectra and (C,D) EDX spectra of (A, C) Al_2O_3 NPs, (B, D) Al_2O_3-SH.

The grafting amount of MPTMS attached onto the Al_2O_3-SH was determined by TGA. Figure 3 shows the thermal decomposition behaviors of Al_2O_3 NPs and Al_2O_3-SH. The weight loss of pure Al_2O_3 was found to be ca. 8.1% when heated from room temperature to 800 ^oC, which may be assigned due to the weight loss for the hydroxyl groups or adsorbed gases on Al_2O_3 NPs. The MPTMS modified Al_2O_3 (Al_2O_3-SH) lost 13.5% weight at the temperature range of 50 ^oC and 800 ^oC, thus, the content of the grafted coupling agent onto Al_2O_3 NPs is close to the value of 5.4 wt%, as estimated from the TGA curve in Figure 3B.

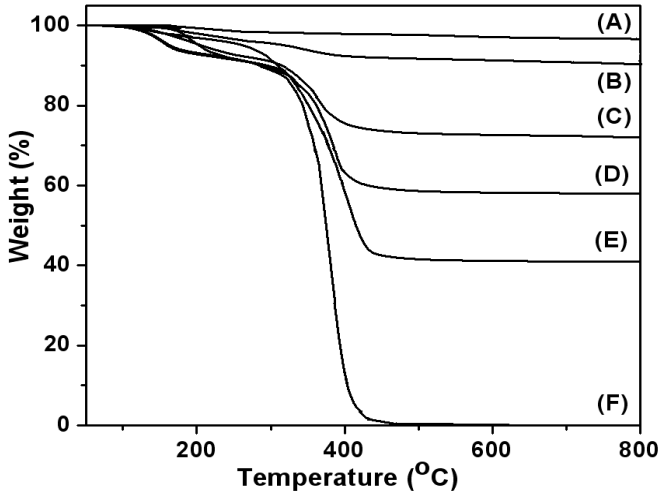

Figure 3. TGA scans of (A) Al_2O_3 NPs, (B) Al_2O_3-SH, (C, D and E) PMMA-*g*-Al_2O_3 after polymerization for 5 h, 10 h, and 15 h, respectively, and (F) cleaved PMMA from PMMA-*g*-Al_2O_3.

3.2 Surface thiol-lactam initiated radical polymerization of MMA from Al_2O_3 *NPs surface*

MPTMS immobilized Al_2O_3 NPs were utilized as initiators for TLIRP, where BL was used as a radical generating agent for the polymerization. FT-IR spectroscopy studies yielded useful qualitative information of the PMMA-*g*-Al_2O_3 nanocomposites as shown in Figure 1C. The covalently anchored PMMA with Al_2O_3-SH was observed by a new band appeared at around 1730 cm^{-1} which indicates the characteristic C=O double bond stretching of PMMA. The absorption bands in the range of 3000 to 2800 cm^{-1} may ascribe to C-H stretching vibrations

of the CH_3 and CH_2 groups of PMMA on the surface of Al_2O_3 NPs. These results imply that the PMMA was successfully grafted on the surface of Al_2O_3 NPs.

The structure and morphology of PMMA-*g*-A_2O_3 nanocomposites were characterized using SEM analysis as shown in Figure 4. The crystalline structure of Al_2O_3 NPs is easily recognized from the FE-SEM image (Fig. 4A). Grafting of PMMA onto the Al_2O_3 NPs can be observed as a soft polymer layer by taking a close look onto the FE-SEM image of PMMA-*g*-A_2O_3 nanocomposites (Fig. 4B). The changes obviously happened because of the anchoring of PMMA brushes onto the surface of the Al_2O_3 NPs. It is observed that there is no aggregation of a large quantity of NPs in the PMMA-*g*-A_2O_3 nanocomposites. Most of the NPs are distributed individually. It is rational that upon modification by polymer, the surface energy of NPs decreased and the aggregation among NPs consequently decreased. These images confirmed the homogeneous dispersion of modified Al_2O_3 NPs in the PMMA matrix. It is thus concluded that the modified nanoparticles had a better dispersion property than the bare Al_2O_3 NPs. In order to obtain information on the size and size distribution of Al_2O_3 NPs, the DLS measurement was undertaken as shown in Figure 4C,D. It is clearly revealed that the average size of Al_2O_3 NPs is larger than that of PMMA-*g*-Al_2O_3 nanocomposites. A number of aggregations were visualized in the aqueous system of unmodified Al_2O_3 NPs (Fig. 4C), so the mean size reflected the aggregation of several Al_2O_3 NPs. On the contrary, Figure 4D shows almost homogeneous size distribution of Al_2O_3 NPs in polymer matrix. This result is good agreement with that of SEM results. Above findings clearly illustrate that covalent grafting of PMMA *via* surface TLIRP play important roles in the dispersion of Al_2O_3 NPs.

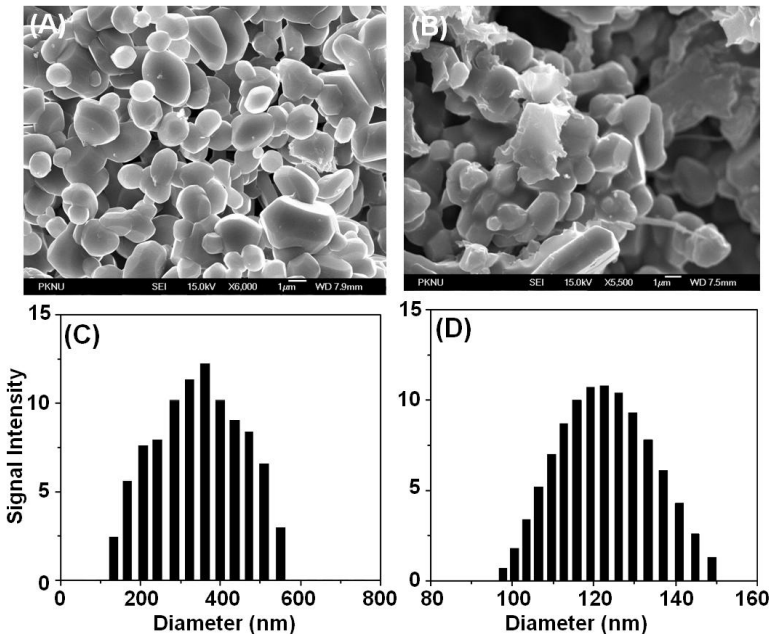

Figure 4. (A, B) SEM images and (C, D) Size distribution of (A, C) Al_2O_3 NPs, and (B, D) PMMA-*g*-Al_2O_3 nanocomposites.

Controlled nature of the polymerization is generally characterized by a linear increase of the molecular weight with conversion and reaction time, and a narrow molecular weight distribution as evidenced by a polydispersity index (PDI = M_w/M_n). Employing TLIRP, controlled radical polymerization from the surface of A_2O_3-SH NPs were attempted for different reaction times ranging from 5 to 15 h. Figure 5A shows the changes of M_n and the PDI's with monomer conversion, as the conversions being determined gravimetrically. The monomer conversion was reached at ca. 62.4% after carrying out the polymerization for 15 h.

By GPC analysis, it was observed that the molecular weight of PMMA increased with increasing monomer conversion, and the molecular weight of the grafted polymer could be tuned with the polymerization time. Figure 5B shows the GPC elution profiles of the cleaved PMMA from PMMA-*g*-Al_2O_3 nanocomposites (5-15 h polymerization time) using HCl. The molecular weights distributions are found to be unimodal and narrow.

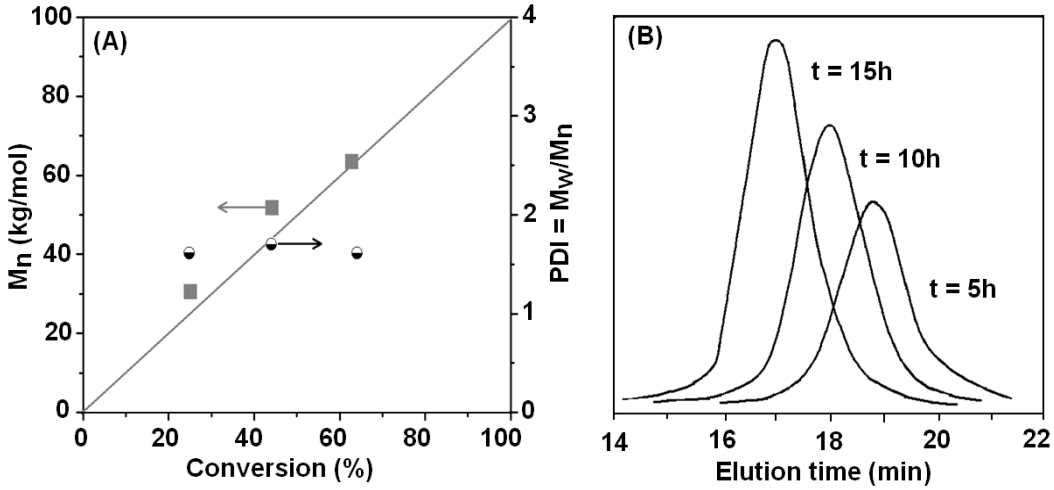

Figure 5. (A) Molecular weight, PDI/conversion data and (B) GPC elution profiles for PMMA brushes were cleaved from PMMA-*g*-Al_2O_3 nanocomposites using HCl.

To examine the compositional effect on the thermal behavior of PMMA-*g*-Al_2O_3 nanocomposites, TGA analysis was undertaken for all the samples at the temperature range from 50 to 800 ^oC. As shown in Figure 3C-E, the amount of polymer on Al_2O_3 NPs surface increases with polymerization time. TGA curve of PMMA-*g*-Al_2O_3 nanocomposites shows a major decomposition at the temperature from 250 to 430 ^oC corresponding to deposition of PMMA on the Al_2O_3 NPs surface. The weight loss of PMMA-*g*-Al_2O_3 nanocomposites is estimated to be 30.6% after polymerization for 5 h (Figure 3C) and approached to 62.7% after polymerization for 15 h (Figure 3E). The PMMA decomposed completely at about 420 ^oC as shown in Figure 3F. The grafting amount of the polymer was calculated from the TGA curve which demonstrates a moderate degree of functionalization of Al_2O_3 NPs by PMMA.

An improved glass transition temperature (*Tg*) of the nanocomposites was observed for all the PMMA-*g*-Al_2O_3 samples when compared with the pure PMMA. Figure 6 shows the *Tg* values of the pure PMMA and the PMMA grafted Al_2O_3 NPs as investigated by DSC. The pure PMMA exhibited a heat flow change at *ca*. 108.7 ^oC, corresponding to the characteristic *Tg* of PMMA. On the other hand, the *Tg* of PMMA-*g*-Al_2O_3 nanocomposites at different polymerization time of 5, 10 and 15 h were found to be 116.4 ^oC, 119.2 ^oC, and 123.7 ^oC, respectively. It was observed that *Tg* of PMMA-*g*-Al_2O_3 nanocomposites improved in accordance with the increased amount of PMMA. The reason behind the increase of *Tg* can be explained in such a way that the confining of one end of the PMMA chains on the Al_2O_3 NPs would restrict the movement and vibration of the whole chain which developed strong interaction as well as the inherent high modulus of Al_2O_3 NPs resulting in increased *Tg*. All of the results suggest that thermal property of PMMA enhanced upon inclusion of Al_2O_3 NPs.

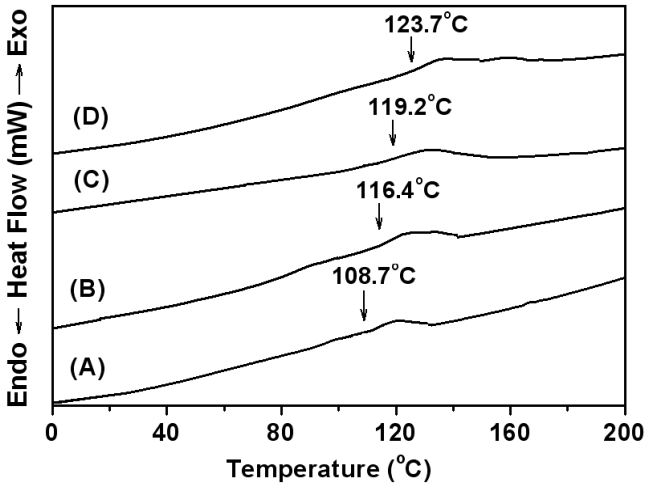

Figure 6. DSC curves of (A) PMMA, PMMA-*g*-Al_2O_3 nanocomposites after polymerization time of (B) 5 h, (C) 10 h, and (D) 15 h, respectively.

The physical structure of the Al_2O_3 NPs, Al_2O_3-SH and PMMA-*g*-Al_2O_3 nanocomposites was investigated by XRD pattern as shown in Figure 7. The diffracted curves of Al_2O_3 NPs exhibit (Fig. 7A) several sharp peaks at 2θ regions of 25.7°, 35.2°, 37.9°, 43.4°, 52.6°, 57.6°, 61.4°, 66.5° and 68.2° which are good agreement with the crystalline structure of Al_2O_3 NPs. As shown in Figure 7B-E, the characteristic diffraction peaks of the (012), (104), (113), (024), (116), (018), (124), and (300) are correspond to the crystal planes of Al_2O_3-SH and PMMA-*g*-Al_2O_3 nanocomposites which are almost identical with the XRD patterns of Al_2O_3 NPs. This result suggests that the grafting of PMMA did not alter the crystallinety or did not form any secondary phase due to chemical reaction and/or maintenance of crystallinety of Al_2O_3 NPs.

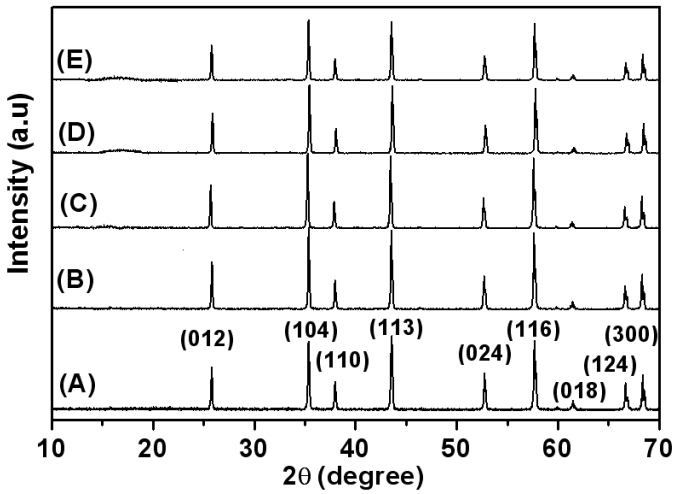

Figure 7. XRD patterns of (A) Al_2O_3 NPs, (B) Al_2O_3-SH, PS-*g*-Al_2O_3 nanocomposites after polymerization time of (C) 5 h, (D) 10 h, (E) 15 h, respectively.

3 Conclusions

PMMA anchored Al_2O_3 nanoparticles were successfully synthesized *via* a simple surface thiol-lactam initiated radical polymerization employing *grafting from* protocol. The structure and surface properties of PMMA-*g*-Al_2O_3 nanocomposites were investigated by FT-IR, XPS and EDX. The XRD study suggested that the grafting polymerization did not alter the crystalline structure of Al_2O_3 nanoparticles. Upon inclusion of Al_2O_3 NPs in the PMMA matrix, the thermal property was found to be enhanced from the TGA and DSC analyses. The morphology of the nanocomposites was captured by FE-SEM which revealed that Al_2O_3 NPs

were encapsulated by polymer resulting in a well dispersed matrix. The molecular weight of the cleaved PMMA from Al_2O_3 NPs surface was found to be increased with increasing monomer conversion suggesting controlled nature of the TLIRP.

Acknowledgments
This work was supported by the Korea Science and Engineering Foundation (KOSEF) grant funded by the Korea government (MEST) (No. R01-2008-000-21056-0) and the second stage of the BK21 program.

Reference
[1] Zhao B., Brittain W.J. Polymer brushes: surface-immobilized macromolecules. *Prog. Polym. Sci.*, **25**, 677–710 (2000).
[2] Yu H.J., Luo Z.H. Novel superhydrophobic silica/poly(siloxane-fluoroacrylate) hybrid nanoparticles prepared *via* two-step surface-Initiated ATRP: synthesis, characterization, and wettability. *J. Polym. Sci. Part A: Polym. Chem*., **48**, 5570–5580 (2010).
[3] Park J.T., Koh J.H., Koh J.K., Kim J.H. Surface-initiated atom transfer radical polymerization from TiO_2 nanoparticles. *Appl. Surf. Sci*., **255**, 3739–3744 (2009).
[4] Bach L.G., Islam M.R., Jeong Y.T., Gal Y.S., Lim K.T. Synthesis and characterization of chemically anchored adenosine with PHEMA grafted gold nanoparticles. *Appl. Surf. Sci.*, **258**, 2816–2822 (2012).
[5] Roth P.J., Theato P. Versatile synthesis of functional gold nanoparticles: grafting polymers from and onto. *Chem. Mater.*, **20**, 1614–1621 (2008).
[6] Matsuno R., Yamamoto K., Otsuka H., Takahara A. Polystyrene-grafted magnetite nanoparticles prepared through surface-initiated nitroxyl-mediated radical polymerization. *Chem. Mater.*, **15**, 3-5 (2003).
[7] Ngo V.G., Bressy C., Leroux C., Margaillan A. Synthesis of hybrid TiO_2 nanoparticles with well-defined poly(methyl methacrylate) and poly(tert-butyldimethylsilyl methacrylate) *via* the RAFT process. *Polymer*, **50**, 3095–3102 (2009).
[8] Plunkett K.N., Zhu X., Moore J.S., Leckband D.E. PNIPAM Chain Collapse Depends on the Molecular Weight and Grafting Density. *Langmuir*, **22**, 4259-4266 (2006)
[9] Zhou F., Liu W., Chen M., Sun D.C. A novel way to prepare ultra-thin polymer films through surface radical chain-transfer reaction. *Chem. Commun.*, **23**, 2446-2447(2001).
[10] Hwang H.S., Bae J.H., Kim H.G., Lim K.T. Synthesis of silica–polystyrene core–shell nanoparticles *via* surface thiol-lactam initiated radical polymerization. *Eur. Polym. J*., **46**, 1654–1659 (2010).
[11] Rashid M.H., Bae J.H., Park C., Lim K.T. Synthesis of well-dispersed multiwalled carbon nanotubes-polystyrene nanocomposites *via* surface thiol-lactam initiated radical polymerization. *Mol. Cryst. Liq. Cryst*., **532**, 514–521 (2010).
[12] Bach L.G., Islam M.R., Kim J.T., Seo S.Y., Lim K.T. Encapsulation of Fe_3O_4 magnetic nanoparticles with poly(methyl methacrylate) via surface functionalized thiol-lactam initiated radical polymerization. *Appl. Sur. Sci*., **258**, 2959–2966 (2012).